This version is the accepted version of the article published in Advanced Materials Interfaces. The final published version is available online at: **DOI: 10.1002/admi.201700755**

X-ray absorption spectroscopy of TiO_2 nanoparticles in water using a holey membrane-based flow cell

Tristan Petit, Jian Ren, Sneha Choudhury, Ronny Golnak, Sreeju S. N. Lalithambika, Marc F. Tesch, Jie Xiao, Emad F. Aziz*

Dr. T. Petit, J. Ren, S. Choudhury, Dr. R. Golnak, S. S. N. Lalithambika, Dr. M. F. Tesch, Dr. J. Xiao, Prof. E. F. Aziz
Methods for Material Development, Helmholtz-Zentrum Berlin für Materialien und Energie GmbH, Albert-Einstein-Strasse 15, 12489 Berlin, Germany
J. Ren, S. Choudhury, S. S. N. Lalithambika, Prof. E. F. Aziz
Department of Physics, Freie Universität Berlin, Arnimallee 14, 14195 Berlin, Germany
E-mail: tristan.petit@helmholtz-berlin.de

Keywords: X-ray absorption spectroscopy; nanoparticle; solid-liquid interface; solvation; in situ spectroscopy.

Abstract

Many applications of TiO_2 nanoparticles, such as photocatalytic water splitting or water remediation, occur in aqueous environment. However, the impact of solvation on TiO_2 electronic structure remains unclear because only few experimental methods are currently available to probe nanoparticle-water interface. Soft X-ray absorption spectroscopy has been extensively used to characterize the electronic structure of TiO_2 materials, but so far only in vacuum conditions. Here we present oxygen K edge and titanium L edge X-ray absorption spectroscopy characterization of TiO_2 nanoparticles measured directly in aqueous dispersion. For this purpose, we introduce a new method to probe nanomaterials in liquid using a holey membrane-based flow cell. With this approach, the X-ray transmission of the membrane is increased, especially in the water window, compared to solid membranes.

Main Text

TiO_2 nanoparticles are interacting with water molecules for most of their applications in photocatalysis[1] and water remediation,[2] either as a solvent or as an active catalytic reagent. In this regard, water adsorption on TiO_2 nanoparticles has been the topic of intense research efforts.[1,3–5] However, direct spectroscopic measurements at the TiO_2-water interface in aqueous environment, such as provided by infrared spectroscopy[6–8] or X-ray photoelectron spectroscopy (XPS),[9] remain scarce.

Soft X-ray absorption spectroscopy (XAS) is a powerful analytical method probing unoccupied electronic states, which has been extensively applied to TiO_2 nanomaterials in vacuum.[10–19] Its application to liquids and solvated ions has enable significant progress in the understanding of solvation effects.[20–22] Indeed, XAS is element-specific and sensitive to chemical environment therefore contribution from solvent and solute can usually be separated. For example, its application to cobalt,[23] iron[24] and diamond[25,26] nanoparticles dispersed in water have demonstrated that XAS is sensitive to charge transfer, change of oxidation state or solvent reorganization, respectively.

In this work, we characterized TiO_2 nanoparticles dispersed in water by XAS in total fluorescence yield (TFY) using a holey membrane-based flow cell (HMFC). The oxygen K and titanium L edges of aqueous dispersions of anatase TiO_2 nanoparticles stabilized by nitric acid (TiO_2-HNO_3) and mixed anatase/brookite TiO_2 nanoparticles stabilized by tetramethylammonium hydroxide (TiO_2-TMAOH) were characterized using the HMFC and compared to liquid microjet and dry sample measurements. Furthermore, the electronic structure of pure water characterized through holey membranes was also compared to microjet experiment.

Different strategies have been developed to probe liquid samples in the soft X-ray range, where the K edges of light elements and the L edges of transition metals lie, but they remain difficult to apply to nanoparticle dispersions. Liquid microjet enables the direct probing of the

liquid-vacuum interface but large amounts of sample (hundreds of ml) are needed and the nanoparticles have to be well-dispersed to avoid blocking of the microjet nozzle.[9,25,27] Static and flow cell strategies, using ultrathin Si_3N_4 or SiC membranes (generally 100-200 nm thick) to isolate the liquid phase from the vacuum,[28,29] can be applied to smaller amount of samples (<10 ml) and have less stringent requirements concerning the size and stability of the solvated nanomaterials.[23,26] However, the membranes absorb a significant amount of soft X-ray light, especially in the water window, below 535 eV, as shown in **Figure 1a,**[30] which can be an issue to probe dilute nanoparticles.

Graphene-covered holey membranes were recently introduced to isolate liquid from vacuum for X-ray photoelectron spectroscopy (XPS) with an ultrathin graphene layer having excellent X-ray and electron transmissions.[31,32] Transfer of graphene on holey membrane with full coverage of the holes remains however complex and the stability of the graphene layer under X-ray illumination might prevent prolonged measurements.

An alternative approach would be to probe directly the liquid-vacuum interface using a flow cell system. Ion and electron measurements at the liquid-vacuum through a micron-sized hole have already been reported on microfluidic chips, on which a stable liquid-vacuum interface could be maintained by liquid surface tension and the use of a continuous flow.[33–35] This method is however currently limited to sub-micron light sources, which is usually not available for soft X-rays in most of current synchrotron facilities. We propose here to circumvent this limitation using a holey membrane, offering a matrix of holes (50 x 50 holes of 750 nm diameter in this work) where a larger liquid-vacuum interface is exposed to the X-ray beam (**Figure 1b**). We have found that such membranes remained stable over several hours under X-ray illumination, with chamber pressure in the range of 10^{-6} mbar during XAS measurements.

First, the oxygen K edge XAS for pure water, TiO_2-TMAOH and TiO_2-HNO_3 were recorded (**Figure 2a**). TFY measurements using a liquid microjet and total electron yield (TEY)

measurements on dry TiO_2 nanoparticles are also plotted for comparison. Typical XA spectra at the O K edge of liquid water consist of a pre-edge at 535 eV, a main-edge around 537 eV and a post-edge at 540 eV.[22,36] In the region of 530-534 eV, oxygen signal from the TiO_2 nanoparticles is detected and is well separated from oxygen contribution from water molecules. Oxygen K edge of TiO_2 nanoparticles also present broad bands in the range 538-545 eV as seen on dried samples,[10] which are however screened by the water signal in aqueous dispersions. For microjet measurements, the XA spectra appears saturated above 536 eV due to X-ray self-absorption of water molecules. This effect seems reduced for measurements performed in the HMFC, which might be related to a different position of the photodiode used for TFY measurement. For TiO_2-TMAOH nanoparticles, XA spectra obtained for HMFC and microjet experiments overlap in the pre-edge region. Note that the microjet could not be operated successfully for TiO_2-HNO_3 nanoparticles, probably because of their higher aggregated state.

The pre-edge region of the oxygen K edge has been fitted with Gaussian peaks as shown in **Figure 2b** to better estimate the energy of the various features observed. The energy position and width of the fitted peaks are listed in **Table S1**. An arctangent background was used to take into account the photoionization potential at the oxygen K edge. The second derivatives of the XA spectra were used for the initial guess of peak positions as minimum of the second derivative corresponds to local maximum in the absorption spectrum.[37] More details on the fitting procedure are available in SI.

First, the features related to water molecules are discussed. The pre-edge around 535 eV is related to water molecules with one uncoordinated O-H group and is very sensitive to weak or broken hydrogen bonds.[21,22] For microjet measurement, a single peak at 535.0 eV is observed, as expected from liquid water. On the other hand, for all spectra recorded with the HMFC, two components D and E at around 534.5 eV and 535.3 eV are detected (Figure 2),

suggesting significant distortions of the water hydrogen bond network in the HMFC compared to microjet.

The relatively long exposure of water molecules to the vacuum (estimated to ~2 ms), due to a smaller liquid flow than for microjet by three orders of magnitude, would lead to a significant temperature drop at the liquid-vacuum interface.[38,39] This temperature drop would potentially lead to the formation of an ice layer at the liquid-vacuum interface, although stable liquid water below the freezing point was also reported for water droplets under evaporative cooling.[39]

Hexagonal ice has been previously characterized and its XA spectrum presents an intense post-edge due to enhanced hydrogen bonding between water molecules.[21,40–42] Such enhancement of the post-edge is clearly not observed for HFMC measurements therefore the formation of an extended hexagonal ice layer at the liquid-water interface can be ruled out. On the other hand, Tse *et al.* have reported that XA of high density amorphous (HDA) ice resembles liquid water with an upshifted pre-edge.[41] Formation of HDA ice generally necessitates low temperature and high pressures, but supercooled water on BaF_2(111) at low pressure was also found to have similar XA spectra.[43]

The water XA spectrum measured with the HMFC resembles a superposition of HDA ice (feature F) and liquid water (feature E) signatures, shifted of +0.3 eV and -0.5 eV, respectively, compared to liquid water measured with a microjet. The energy up-/downshifts might potentially be related to an in-/decrease in the water density in the HDA ice or supercooled liquid and liquid phases, respectively. Precise estimation of the surface temperature in the holes,[38,39] and the use of surface-sensitive X-ray spectroscopy, such as XPS, would nevertheless be required to gain further insights into the water structure induced by the liquid-vacuum interface in HMFC. In any case, TiO_2 nanoparticles dispersions could flow through the HMFC and were effectively removed from the cell after flowing pure water, showing that the nanoparticles were not trapped in any ice layer.

The pre-edge associated to TiO_2 nanoparticles at 530-534 eV is composed of three or four features, which are not detected in pure water (Figure 2b). Peaks B and D are related to oxygen 2p states hybridized with the unoccupied Ti 3d bands, splitted into t_{2g} and e_g components due to ligand-field effects.[10,12] For TiO_2-HNO_3, t_{2g} and e_g states appears at 530.8 eV and 533.4 eV, respectively, demonstrating a field splitting of 2.6 eV as reported on bulk TiO_2.[10] These peaks are broad (Full Width at Half Maximum of 1.3 eV and 1.4 eV, respectively, compared to 1.0 eV for water-related peaks) which may be due to the small size and the polydispersity of the nanoparticles.[18] The feature C appearing at 532.05 eV is related to HNO_3 molecules used as stabilizer.[44] These three features are also observed on dried sample, with a reduced intensity for C because of evaporation of the stabilizer in vacuum (see Figure S2).

For TiO_2-TMAOH nanoparticles, the peaks B and D, related to t_{2g} and e_g components, are upshifted of +0.3 eV compared to TiO_2-HNO_3, which might result from the smaller size of TiO_2-TMAOH nanoparticles (2-5 nm instead of 4-8 nm). A similar upshift of the t_{2g} band was observed on TiO_2 deposited on SnO_2:F, associated to structural distortions induced by the interface.[45] Furthermore, a low-energy pre-edge A at 530.25 eV is detected on TiO_2-TMAOH. This feature A may be related to local structural distortion of the Ti-O bonds induced by strong hydrogen bonding with water molecules.[47,48] Hydrogen bonding between Ti surface atoms and neighbouring molecules could decrease the Ti-O bond covalency of surface atoms.[3] The formation of distorted Ti-O bonds would inducing the appearance of a lower energy peak at the oxygen K edge, as also observed for distorted Co-O bonds induced by the de-intercalation of Li^+ ions on $LiCoO_2$ materials.[49] This feature is not as clearly detected for TiO_2-HNO_3, probably due to their larger crystallite sizes, although the slight broadening of the feature B compared to the dry sample may result from similar solvation effect. Finally, the peak C at 532.5 eV is related to hydroxide ions from TMAOH used as stabilizer as a similar feature was previously observed in concentrated KOH solutions.[46]

Dry TiO_2-TMAOH nanoparticles have a completely different signature from the solvated ones, suggesting a structural rearrangement of the nanoparticles after drying. In particular, the splitting into the t_{2g} and e_g peaks is not visible anymore. Similar effect was reported by Kronawitter *et al* for sub-5 nm amorphous Ti_xO_y layer on Fe_2O_3.[15] Most probably, the TiO_2-TMAOH nanoparticles reconstruct into an amorphous film upon drying due to the small size of the crystallites. TiO_2-TMAOH nanoparticles seem to be stabilized by interaction with water molecules in their hydration shell, inducing slight distortions of Ti-O bonds at the solid-liquid interface.

Ti L edge of the TiO_2 nanoparticles was also characterized and dry and liquid measurements are compared (**Figure 3**). Characteristic features of L_2 (463-468 eV) and L_3 (458-462 eV) edges, including the splitting of both contributions into two main components related to t_{2g} and e_g states are observed.[11–14,19] The relative intensities of the XA features recorded on dry and dispersed TiO_2 nanoparticles differ and the peaks are broadened for aqueous dispersions, especially the pre-edge around 457 eV and the $L_2(e_g)$ state. An energy shift of approximately + 0.2 eV of the $L_2(e_g)$ state is also observed for the dispersed nanoparticles. When dispersed in water, recent XPS experiments have demonstrated that a downward band bending of 250 meV may occur at the surface of TiO_2 nanoparticles.[9] A change in the electronic environment at the surface of TiO_2 nanoparticles is likely to change their oxidation state, which has been shown to induce an energy shift of the $L_2(e_g)$ state. [15] Having diameters below 8 nm, TiO_2 nanoparticles used in this study would be particularly sensitive to surface band bending, and the peak broadening might result from overlapping contributions from core and surface Ti atoms. For TiO_2-TMAOH, the reduced intensity of the L_3 peaks on dry sample, in particular the $L_3(t_{2g})$ that becomes smaller than the $L_3(e_g)$, cannot be imputed only to solvation effect. This XA spectrum is close to Ti L edge of amorphous TiO_2,[13] confirming the instability of this sample upon drying.

In summary, we have successfully characterized TiO_2 nanoparticles in water with XAS at the oxygen K and titanium L edges through a holey membrane. Hydration induces a broadening of Ti L edge features and the appearance of a shoulder in the pre-edge of oxygen K edge, which we attributed to distorted Ti-O bonds induced by hydrogen bonding with water molecules. These interactions with water molecules may stabilize the smallest TiO_2 nanoparticles, which have an electronic signature similar to amorphous films when dried in vacuum. XA spectra of pure water recorded with the HMFC differ from pure liquid signature and further experiments are required to understand the water structure at the liquid-vacuum interface. We anticipate that the use of holey membrane will facilitate the characterization of nanomaterials in solution by soft X-ray spectroscopies, in particular for X-ray excitation energies lying in the water window.

References

[1] M. A. Henderson, *Surf. Sci. Rep.* **2011**, *66*, 185.

[2] M. N. Chong, B. Jin, C. W. K. Chow, C. Saint, *Water Res.* **2010**, *44*, 2997.

[3] Y. He, A. Tilocca, O. Dulub, A. Selloni, U. Diebold, *Nat. Mater.* **2009**, *8*, 585.

[4] S. Benkoula, O. Sublemontier, M. Patanen, C. Nicolas, F. Sirotti, A. Naitabdi, F. Gaie-Levrel, E. Antonsson, D. Aureau, F.-X. Ouf, S.-I. Wada, A. Etcheberry, K. Ueda, C. Miron, *Sci. Rep.* **2015**, *5*, 15088.

[5] J. Matthiesen, J. Ø. Hansen, S. Wendt, E. Lira, R. Schaub, E. Lægsgaard, F. Besenbacher, B. Hammer, *Phys. Rev. Lett.* **2009**, *102*, 226101.

[6] P. A. Connor, K. D. Dobson, A. J. Mcquillan, *Langmuir* **1999**, 2402.

[7] R. Nakamura, A. Imanishi, K. Murakoshi, Y. Nakato, *J. Am. Chem. Soc.* **2003**, *125*, 7443.

[8] H. Belhadj, A. Hakki, P. K. J. Robertson, D. W. Bahnemann, *Phys. Chem. Chem. Phys.* **2015**, *17*, 22940.

[9] M. J. Makowski, R. P. Galhenage, J. Langford, J. C. Hemminger, *J. Phys. Chem. Lett.* **2016**, *7*, 1732.

[10] F. M. F. de Groot, M. Grioni, J. C. Fuggle, J. Ghijsen, G. A. Sawatzky, H. Petersen, *Phys. Rev. B* **1989**, *40*, 5715.

[11] F. M. F. de Groot, M. O. Figueiredo, M. J. Basto, M. Abbate, H. Petersen, J. C. Fuggle, *Phys. Chem. Miner.* **1992**, *19*, 140.

[12] R. Ruus, A. Kikas, A. Saar, A. Ausmees, E. Nõmmiste, J. Aarik, A. Aidla, T. Uustare, I. Martinson, *Solid State Commun.* **1997**, *104*, 199.

[13] S. O. Kucheyev, T. van Buuren, T. F. Baumann, J. H. Satcher, T. M. Willey, R. W. Meulenberg, T. E. Felter, J. F. Poco, S. A. Gammon, L. J. Terminello, *Phys. Rev. B* **2004**, *69*, 245102.

[14] K. E. Lee, M. A. Gomez, T. Regier, Y. Hu, G. P. Demopoulos, *J. Phys. Chem. C* **2011**, *115*, 5692.

[15] C. X. Kronawitter, J. R. Bakke, D. A. Wheeler, W.-C. Wang, C. Chang, B. R. Antoun, J. Z. Zhang, J. Guo, S. F. Bent, S. S. Mao, L. Vayssieres, *Nano Lett.* **2011**, *11*, 3855.

[16] X. Chen, P.-A. Glans, X. Qiu, S. Dayal, W. D. Jennings, K. E. Smith, C. Burda, J. Guo, *J. Electron Spectros. Relat. Phenomena* **2008**, *162*, 67.

[17] X. Chen, L. Liu, Z. Liu, M. A. Marcus, W.-C. Wang, N. A. Oyler, M. E. Grass, B. Mao, P.-A. Glans, P. Y. Yu, J. Guo, S. S. Mao, *Sci. Rep.* **2013**, *3*, 1510.

[18] L. Vayssieres, C. Persson, J.-H. Guo, *Appl. Phys. Lett.* **2011**, *99*, 183101.

[19] R. Brydson, H. Sauer, W. Engel, J. M. Thomass, E. Zeitler, N. Kosugi, H. Kuroda, *J. Phys. Condens. Matter* **1989**, *1*, 797.

[20] K. M. Lange, E. F. Aziz, *Chem. Soc. Rev.* **2013**, *42*, 6840.

[21] A. Nilsson, D. Nordlund, I. Waluyo, N. Huang, H. Ogasawara, S. Kaya, U. Bergmann, L.-Å. Näslund, H. Öström, P. Wernet, K. J. Andersson, T. Schiros, L. G. M. Pettersson, *J. Electron Spectros. Relat. Phenomena* **2010**, *177*, 99.

[22] P. Wernet, D. Nordlund, U. Bergmann, M. Cavalleri, M. Odelius, H. Ogasawara, L. A. Näslund, T. K. Hirsch, L. Ojamäe, P. Glatzel, L. G. M. Pettersson, A. Nilsson, *Science* **2004**, *304*, 995.

[23] H. Liu, Y. Yin, A. Augustsson, C. Dong, J. Nordgren, C. Chang, P. Alivisatos, G. Thornton, D. F. Ogletree, F. G. Requejo, F. de Groot, M. Salmeron, *Nano Lett.* **2007**, *7*, 1919.

[24] Y. Yao, Y. Hu, R. W. J. Scott, *J. Phys. Chem. C* **2014**, *118*, 22317.

[25] T. Petit, M. Pflüger, D. Tolksdorf, J. Xiao, E. F. Aziz, *Nanoscale* **2015**, *7*, 2987.

[26] T. Petit, H. Yuzawa, M. Nagasaka, R. Yamanoi, E. Osawa, N. Kosugi, E. F. Aziz, *J. Phys. Chem. Lett.* **2015**, *6*, 2909.

[27] M. A. Brown, R. Seidel, S. Thürmer, M. Faubel, J. C. Hemminger, J. A. van Bokhoven, B. Winter, M. Sterrer, *Phys. Chem. Chem. Phys.* **2011**, *13*, 12720.

[28] B. X. Yang, J. Kirz, *Phys. Rev. B* **1987**, *36*, 1361.

[29] J. Guo, T. Tong, L. Svec, J. Go, C. Dong, J.-W. Chiou, *J. Vac. Sci. Technol. A Vacuum, Surfaces, Film.* **2007**, *25*, 1231.

[30] B. L. Henke, E. M. Gullikson, J. C. Davis, *At. Data Nucl. Data Tables* **1993**, *54*, 181.

[31] A. Kolmakov, D. A. Dikin, L. J. Cote, J. Huang, M. K. Abyaneh, M. Amati, L. Gregoratti, S. Günther, M. Kiskinova, *Nat. Nanotechnol.* **2011**, *6*, 651.

[32] J. J. Velasco-Velez, V. Pfeifer, M. Hävecker, R. S. Weatherup, R. Arrigo, C.-H. Chuang, E. Stotz, G. Weinberg, M. Salmeron, R. Schlögl, A. Knop-Gericke, *Angew. Chemie Int. Ed.* **2015**, *54*, 14554.

[33] M. Brivio, N. R. Tas, M. H. Goedbloed, H. J. G. E. Gardeniers, W. Verboom, A. van den Berg, D. N. Reinhoudt, *Lab Chip* **2005**, *5*, 378.

[34] L. Yang, X.-Y. Yu, Z. Zhu, M. J. Iedema, J. P. Cowin, *Lab Chip* **2011**, *11*, 2481.

[35] L. Yang, X.-Y. Yu, Z. Zhu, T. Thevuthasan, J. P. Cowin, *J. Vac. Sci. Technol. A Vacuum, Surfaces, Film.* **2011**, *29*, 61101.

[36] L.-A. Näslund, D. C. Edwards, P. Wernet, U. Bergmann, H. Ogasawara, L. G. M. Pettersson, S. Myneni, A. Nilsson, *J. Phys. Chem. A* **2005**, *109*, 5995.

[37] J. A. Sellberg, S. Kaya, V. H. Segtnan, C. Chen, T. Tyliszczak, H. Ogasawara, D. Nordlund, L. G. M. Pettersson, A. Nilsson, *J. Chem. Phys.* **2014**, *141*, 34507.

[38] J. D. Smith, C. D. Cappa, W. S. Drisdell, R. C. Cohen, R. J. Saykally, *J. Am. Chem. Soc.* **2006**, *128*, 12892.

[39] J. A. Sellberg, C. Huang, T. A. McQueen, N. D. Loh, H. Laksmono, D. Schlesinger, R. G. Sierra, D. Nordlund, C. Y. Hampton, D. Starodub, D. P. DePonte, M. Beye, C. Chen, A. V Martin, A. Barty, K. T. Wikfeldt, T. M. Weiss, C. Caronna, J. Feldkamp, L. B. Skinner, M. M. Seibert, M. Messerschmidt, G. J. Williams, S. Boutet, L. G. M. Pettersson, M. J. Bogan, A. Nilsson, *Nature* **2014**, *510*, 381.

[40] S. Myneni, Y. Luo, L. Å. Näslund, M. Cavalleri, L. Ojamäe, H. Ogasawara, A. Pelmenschikov, P. Wernet, P. Väterlein, C. Heske, Z. Hussain, L. G. M. Pettersson, A. Nilsson, *J. Phys. Condens. Matter* **2002**, *14*, L213.

[41] J. S. Tse, D. M. Shaw, G. Vankó, G. Monaco, M. Krisch, *Phys. Rev. Lett.* **2008**, *100*, 95502.

[42] D. Nordlund, H. Ogasawara, K. J. Andersson, M. Tatarkhanov, M. Salmerón, L. G. M. Pettersson, A. Nilsson, *Phys. Rev. B* **2009**, *80*, 233404.

[43] S. Kaya, D. Schlesinger, S. Yamamoto, J. T. Newberg, H. Bluhm, H. Ogasawara, T. Kendelewicz, G. E. Brown, L. G. M. Pettersson, A. Nilsson, *Sci. Rep.* **2013**, *3*, 1074.

[44] A. Křepelová, J. Newberg, T. Huthwelker, H. Bluhm, M. Ammann, *Phys. Chem. Chem. Phys.* **2010**, *12*, 8870.

[45] C. X. Kronawitter, M. Kapilashrami, J. R. Bakke, S. F. Bent, C.-H. Chuang, W.-F. Pong, J. Guo, L. Vayssieres, S. S. Mao, *Phys. Rev. B* **2012**, *85*, 125109.

[46] C. D. Cappa, J. D. Smith, B. M. Messer, R. C. Cohen, R. J. Saykally, *J. Phys. Chem. A* **2007**, *111*, 4776.

[47] M. Sumita, C. Hu, Y. Tateyama, *J. Phys. Chem. C* **2010**, *114*, 18529.

[48] L.-M. Liu, C. Zhang, G. Thornton, A. Michaelides, *Phys. Rev. B* **2010**, *82*, 161415.

[49] W. S. Yoon, K. B. Kim, M. G. Kim, M. K. Lee, H. J. Shin, J. M. Lee, J. S. Lee, C. H. Yo, *J. Phys. Chem. B* **2002**, *106*, 2526.

Experimental Section

Materials: TiO_2-HNO_3 nanoparticles (PL-TiO, Plasmachem GmbH), are composed of anatase phase, with an average particle of 4-8 nm and are stabilized by nitric acid (HNO_3) at a concentration of 10 wt%. TiO_2-TMAOH nanoparticles (PL-TiO-N, Plasmachem GmbH), are made of mixed anatase/brookite phase, with an average particle size of 2-5 nm and stabilized by tetramethylammonium hydroxide (TMAOH) at a concentration of 20 wt%.

Holey membrane-based flow cell measurements: Experiments were conducted at the U49-2_PGM1 undulator beamline of BESSY II synchrotron using the LiXEdrom endstation. Nanoparticles in liquid were characterized in a holey membrane-based flow cell using Total Fluorescence Yield (TFY) recorded with a XUV-100 silicon photodiode (AMS Technologies) in grazing incidence to reduce saturation effect.[36] Holey membranes with 750 nm, 1 µm and 1.25 µm hole sizes on 200 nm silicon nitride membranes were purchased from Ted Pella, Inc. The silicon nitride window has a size of 0.5 x 0.5 mm and the holey area is 75 x 75 µm with a nominal porosity of 22.8 % (50 x 50 holes). In order to ensure a constant pressure of the liquid sample over the membrane during measurement, a Legato 270 syringe pump (KD Scientific Inc.) was used and operated in push-pull mode with a flow of 1 ml/min. The flow also ensure a renewal of probed nanoparticles to avoid samples damage and reduce solvent evaporation in the holes.[35] Good stability of the membrane and good vacuum condition (10^{-6} mbar range) were achieved with 750 nm and 1 µm holey membranes in dark. Under X-ray light exposure, variation in the chamber pressure was observed for 1 µm holey membranes, therefore only 750 nm holey membranes were used for the measurements in this

study. During XAS measurements at O K and Ti L edges, the pressure in the chamber was stable, below 3.10^{-6} mbar, over several hours of measurement. After characterization of the TiO_2 samples, the flow cell was flushed with deionized water and reference spectra were acquired again at the oxygen K edge to validate that no nanoparticles were left in the cell. The energy of the O K edge was calibrated to the water pre-edge at 535.0 eV recorded with the microjet. Since the water pre-edge feature does not appear as a single peak for measurement with the HFMC, the XA spectra at the O K edge for the HMFC were energy calibrated to the pre-edge of TiO_2-TMAOH, which is not influenced by the measurement method. The intensity of the O K edge XA spectra were normalized to the intensities before (528 eV) and after (550 eV) the edge for clarity. The Ti L edge was calibrated to the $L_3(t_{2g})$ feature at 458.3 eV on solid Ti reference (TEY). The intensity of the Ti L edge XA spectra were normalized to the $L_2(t_g)$ peak maximum for clarity.

Microjet measurements: Experiments were conducted at the U41-PGM undulator beamline of BESSY II synchrotron using the LiXEdrom endstation. A 22 µm glass nozzle was used and the pressure in the chamber was ~3.10^{-5} mbar during the microjet measurements. TFY was recorded using a GaAsP photodiode (Hamamatsu) oriented at 45° with respect to the microjet.

Solid measurements: Solid samples were characterized by XAS using Total Electron Yield (TEY) mode on TiO_2 nanoparticles drop casted on a conductive Si substrate at the U49-2_PGM1 and U56-PGM2 beamline of BESSY II.

Supporting Information

Supporting Information is available from the Wiley Online Library or from the author.

Acknowledgements

We thank Florian Gores for technical support in the design of the flow cell and Hebatallah Ali for fruitful discussions. T.P. acknowledges the Volkswagen Foundation (Freigeist Fellowship No. 89592) for financial support. This work was partly supported by European Union's

Horizon 2020 research and innovation programme under Grant Agreement 665085. We acknowledge the kind support by staff members of the BESSY II Synchrotron Facility.

Figure 1. (a) X-ray transmission curves of 100 nm (dashed) and 200nm (solid) silicon nitride, silicon carbide membranes and water equivalent in the soft X-ray range for fluorescence yield measurement. X-ray photons need to pass twice the membrane for fluorescence yield measurement, which was taken into account for the transmission calculation. The energies of the edges relevant to this study are highlighted. (b) Scheme of the holey membrane-based flow cell for total fluorescence yield XAS measurement of TiO_2 nanoparticles. Dimensions are not scaled for clarity.

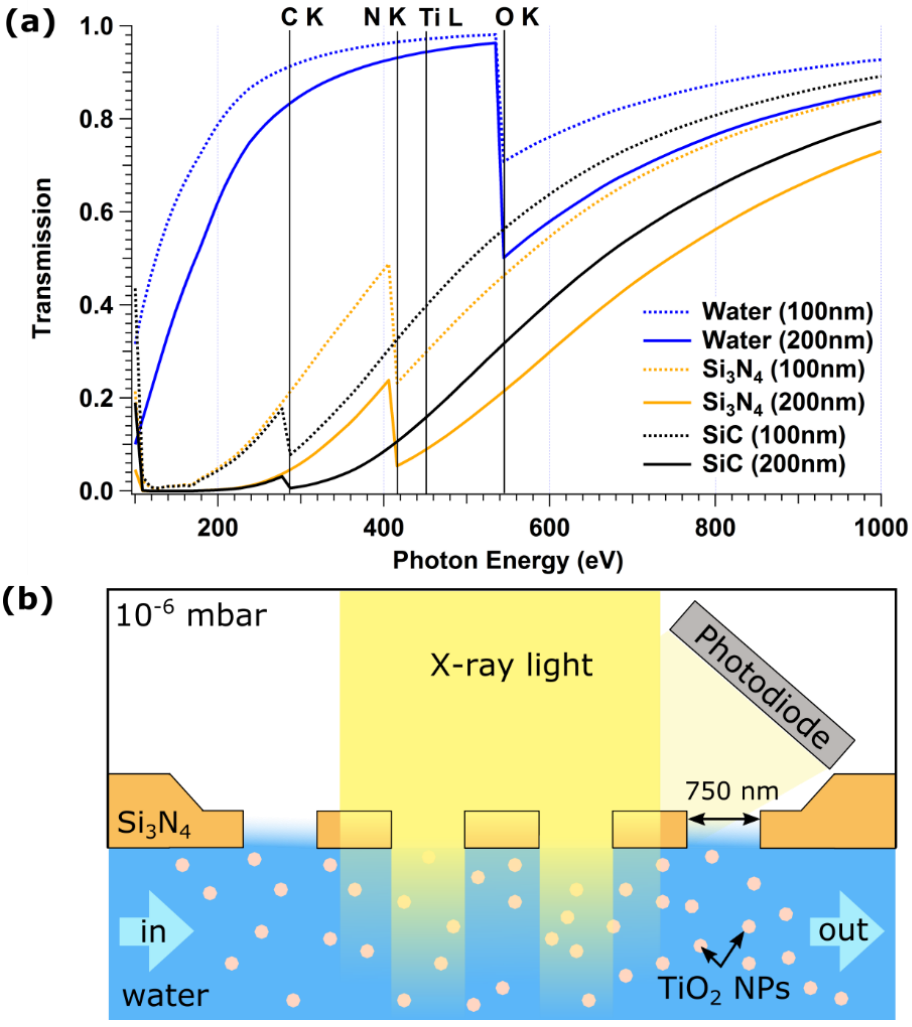

Figure 2. (a) Oxygen K edge XAS of pure water (blue), TiO_2-TMAOH (red) and TiO_2-HNO_3 (black) TiO_2 aqueous dispersions measured with holey membrane-based flow cell (solid), liquid microjet (dashed) and as dry sample (dotted). (b) Deconvolution of the pre-edge features of oxygen K edge XAS. The different Gaussian peaks (solid) and the resulting fit (dashed) are shown below the experimental spectra. The second derivatives of experimental spectra (solid-dotted) are also plotted.

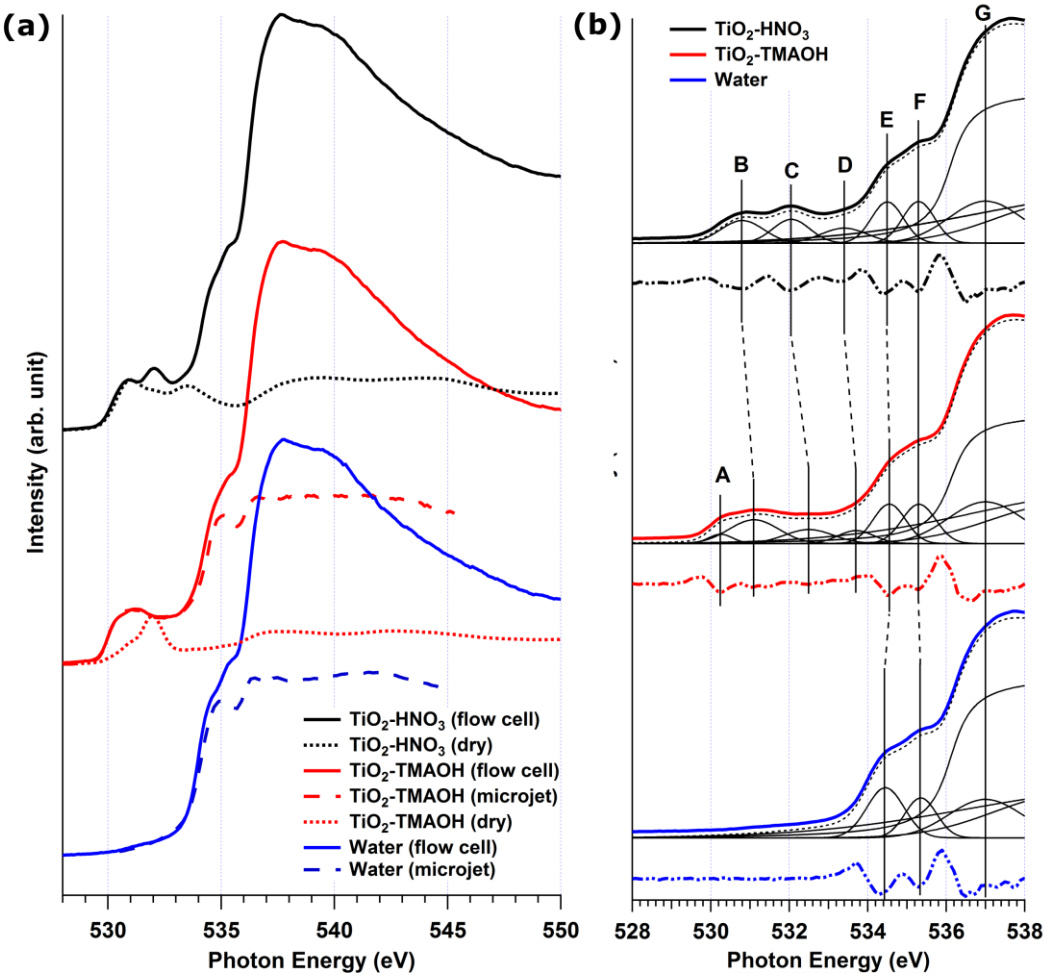

Figure 3. Titanium L edge XAS of TiO_2-TMAOH (red) and TiO_2-HNO_3 (black) aqueous dispersions measured with the holey membrane-based flow cell. XA spectrum recorded with a liquid microjet (dashed) and TEY-XAS of solid samples (dotted) are shown for comparison.

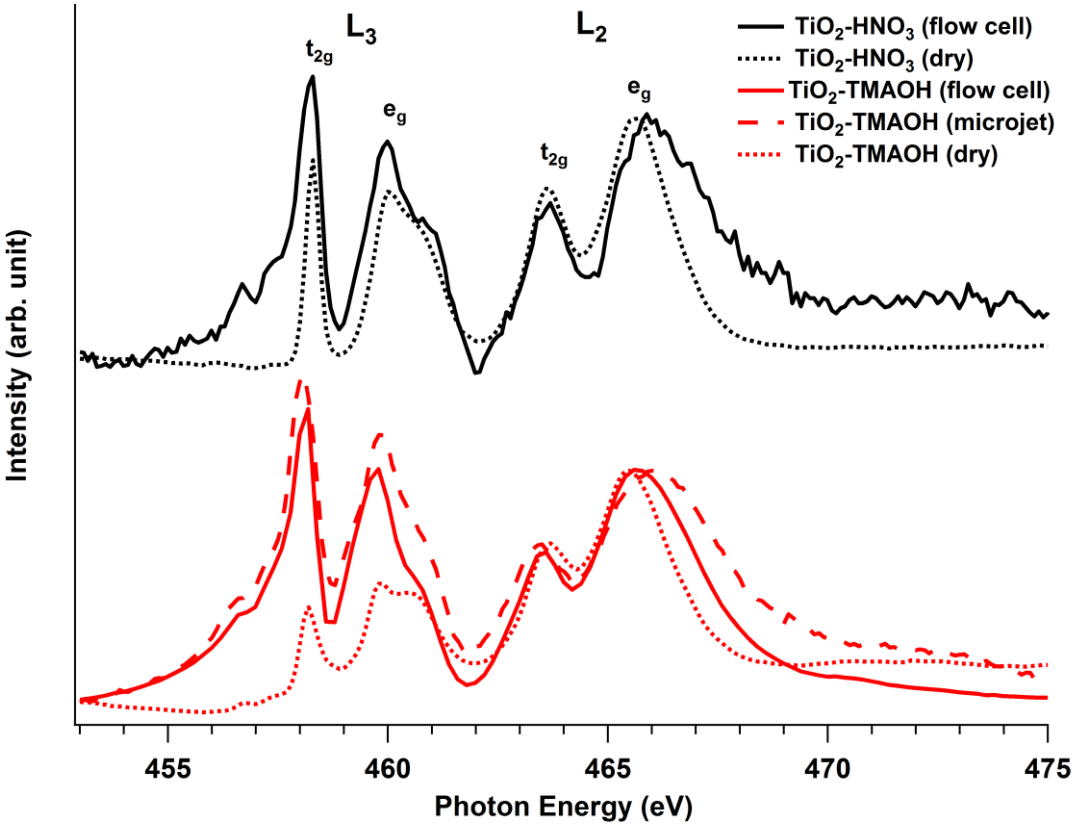

Supporting Information

X-ray absorption spectroscopy of TiO_2 nanoparticles in water using a holey membrane-based flow cell

Tristan Petit, Jian Ren, Sneha Choudhury, Ronny Golnak, Sreeju S. N. Lalithambika, Marc F. Tesch, Jie Xiao, Emad F. Aziz*

Deconvolution procedure of the oxygen K edge spectra

The oxygen K edge XA spectra were fitted using the Multi-peak Fit function of Igor Pro 6.37. The full range spectra are plotted in Figure S1 and the pre-edge is highlighted in Figure 2 of the main article. Pure water XA spectrum was deconvoluted using an arctangent background induced by the ionization potential and five Gaussian peaks. For all samples, the peaks positions of the water contribution were kept constant and their intensities and widths were optimized. Only the parameters for peak E and F were allowed to vary within a small energy range (±0.1 eV), which corresponds to our experimental resolution, to reduce the fitting error. The features above the ionization potential appear extremely broad but we chose to use a minimal number of Gaussian peaks required to have a converging fit. This procedure allows a direct comparison between the water features for the three samples.
For the pre-edge features in the range 530-534 eV, an initial guess of the peak positions was proposed based on the 2nd derivative before optimization of their widths and intensities. For TiO_2-TMAOH sample, initial fits were performed without the peak A, however no satisfactory fit could be obtained in this case. Adding this contribution to fit the XA spectrum of TiO_2-HNO_3 also reduced slightly the fitting error, but we preferred to include the simplest fit to the discussion.

Table S1. Fitting parameters of the oxygen K edge XAS pre-edge of pure water and TiO_2 aqueous dispersions.

Peak component	Water		TiO_2-TMAOH		TiO_2-HNO_3	
	Energy [eV]	FWHM [eV][b)]	Energy [eV]	FWHM [eV]	Energy [eV]	FWHM [eV]
A	-	-	530.25	0.7	-	-
B	-	-	531.1	1.5	530.8	1.3
C	-	-	532.5	1.5	532.05	1.1
D	-	-	533.7	1.1	533.4	1.4
E	534.45	1.1	534.55	1.0	534.5	1.0
F	535.35	1.0	535.3	1.0	535.3	1.0
H	537.0	2.2	537.0	2.2	537.0	2.2
I	539.0	4.3	539.0	4.3	539.0	4.2
J	540.8	10.0	540.8	9.1	540.8	9.3

[b)] Full Width at Half Maximum (FWHM) of Gaussian peaks.

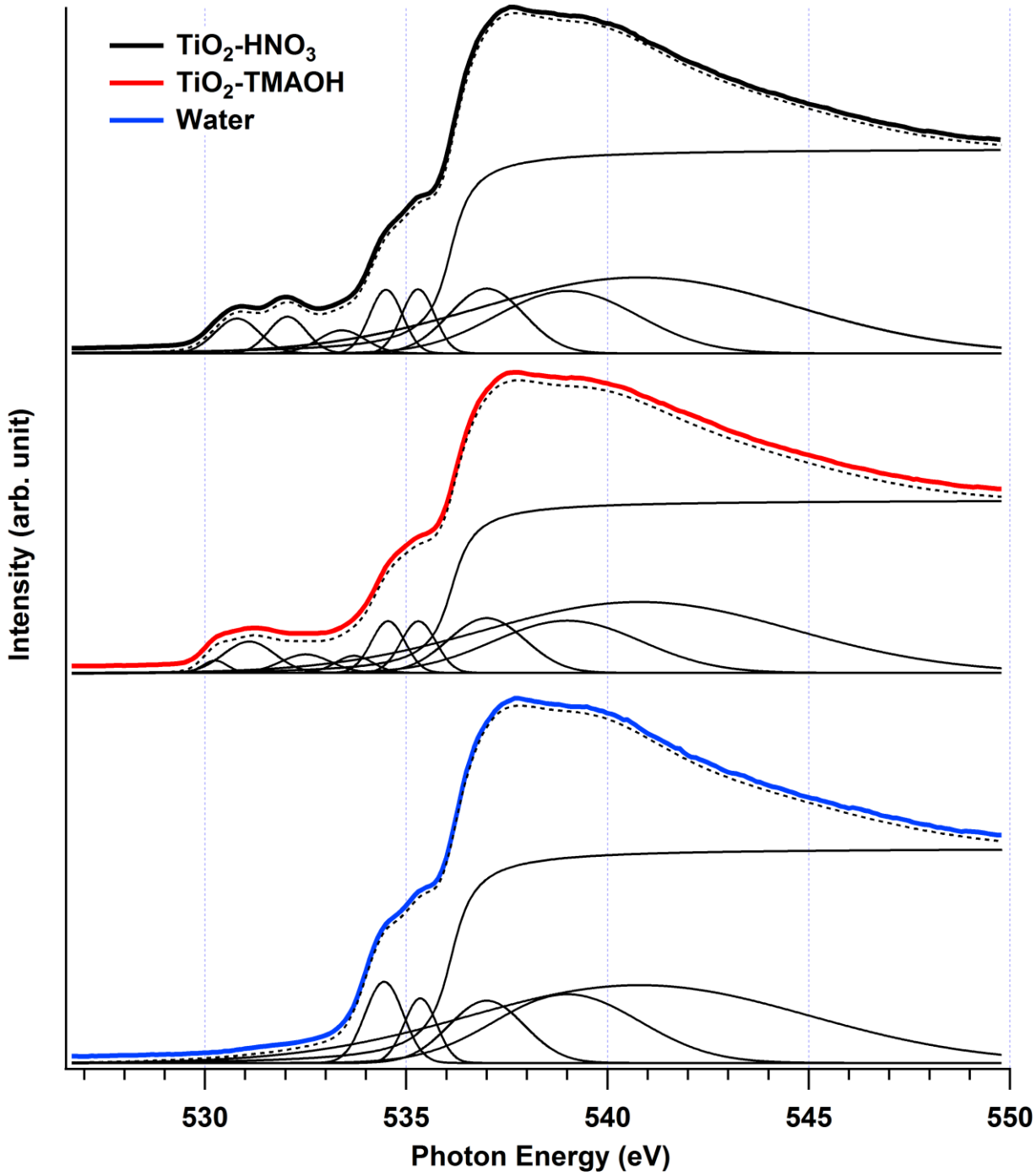

Figure S1. Deconvolution of the oxygen K edge XA spectra of pure water (blue), TiO_2-TMAOH (red) and TiO_2-HNO_3 (black) TiO_2 aqueous dispersions measured with the holey membrane-based flow cell (solid). The different Gaussian peaks and arctan background (solid) and the resulting fit (dashed) are shown below the experimental spectra.

Table S2. Fitting parameters of the oxygen K edge XAS pre-edge of dry TiO_2 nanoparticles.

Peak component	TiO_2-TMAOH		TiO_2-HNO_3	
	Energy [eV]	FWHM [eV]	Energy [eV]	FWHM [eV]
A	530. 5	1.1	-	-
B	531.0	0.7	530.95	1.4
C	531.95	1.1	532.05	0.8
D	533.7	3.0	533.4	2.5
E	536.0	2.3	536.4	3.3
F	538.0	3.0	539.0	6.0
H	542.8	5.6	544.4	4.0

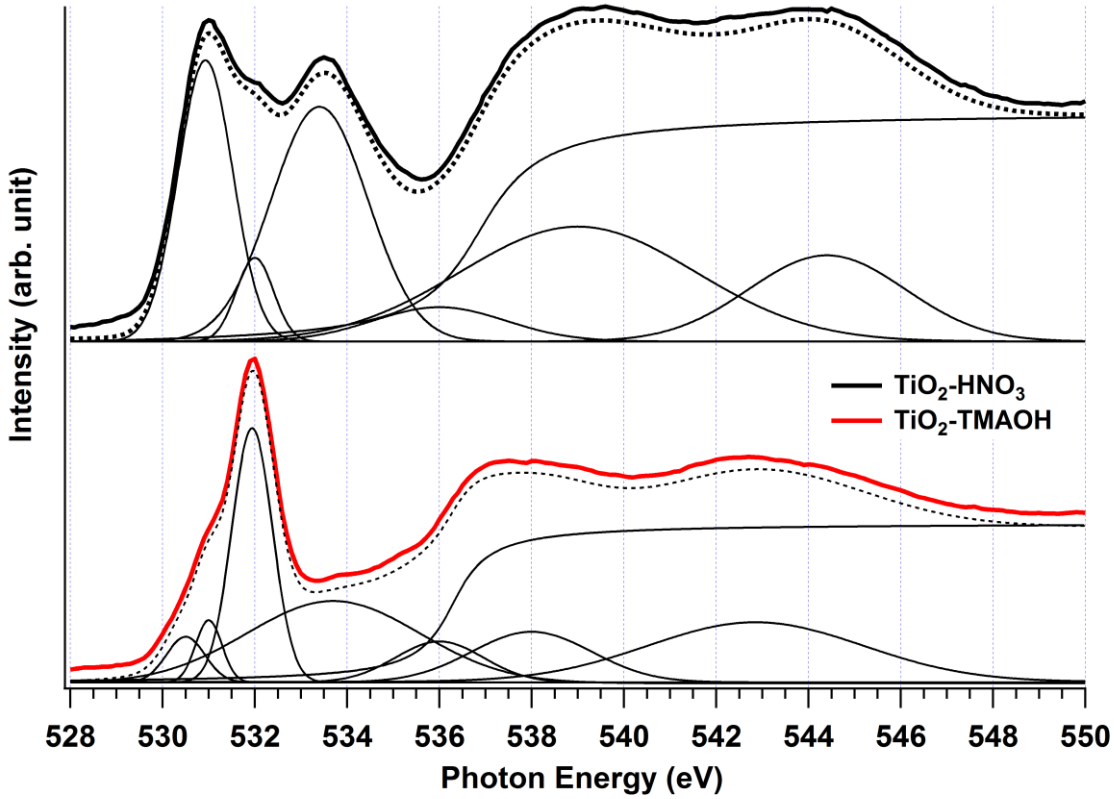

Figure S2. Deconvolution of the oxygen K edge XA spectra of dry TiO_2-TMAOH (red) and TiO_2-HNO_3 (black) TiO_2 nanoparticles (solid). The different Gaussian peaks and arctan background (solid) and the resulting fit (dashed) are shown below the experimental spectra.